OPEN ACCESS



Effective Temperature Estimations from Line Depth Ratios in the *H*- and *K*-band Spectra of IGRINS

Melike Afşar¹, Zeynep Bozkurt¹, Gamze Böcek Topcu¹, Sergen Özdemir^{1,2}, Christopher Sneden³, Gregory N. Mace³, Daniel T. Jaffe³, and Ricardo López-Valdivia⁴

Department of Astronomy and Space Sciences, Ege University, 35100, Bornova, İzmir, Türkiye
 Nicolaus Copernicus Astronomical Center Polish Academy of Sciences, ul. Bartycka 18, 00-716, Warsaw, Poland
 Department of Astronomy and McDonald Observatory, The University of Texas, Austin, TX 78712, USA
 Universidad Nacional Autónoma de México Instituto de Astronomía, AP 106, Ensenada 22800, BC, México Received 2023 January 4; revised 2023 March 13; accepted 2023 March 26; published 2023 June 1

Abstract

Determining accurate effective temperatures of stars buried in the dust-obscured Galactic regions is extremely difficult from photometry. Fortunately, high-resolution infrared spectroscopy is a powerful tool for determining the temperatures of stars with no dependence on interstellar extinction. It has long been known that the depth ratios of temperature-sensitive and relatively insensitive spectral lines are excellent temperature indices. In this work, we provide the first extensive line depth ratio (LDR) method application in the infrared region that encompasses both the H and K bands (1.48 μ m - 2.48 μ m). We applied the LDR method to high-resolution ($R \simeq 45,000$) H- and K-band spectra of 110 stars obtained with the Immersion Grating Infrared Spectrograph. Our sample contained stars with $3200 < T_{\rm eff}$ (K) < 5500, $0.20 \le \log g < 4.6$, and $-1.5 < [{\rm M/H}] < 0.5$. The application of this method in the K band yielded 21 new LDR- $T_{\rm eff}$ relations. We also report five new LDR- $T_{\rm eff}$ relations found in the H-band region, augmenting the relations already published by other groups. The temperatures found from our calibrations provide reliable temperatures within ~ 70 K accuracy compared to spectral $T_{\rm eff}$ values from the literature.

Unified Astronomy Thesaurus concepts: Stellar effective temperatures (1597); Stellar properties (1624); Stellar spectral lines (1630); Infrared spectroscopy (2285)

Supporting material: machine-readable tables

1. Introduction

The effective temperature ($T_{\rm eff}$) is of fundamental importance among stellar atmospheric parameters. Knowing the temperature enables assessment of the mass, age, and surface gravity of stars, as well as estimation of their evolutionary status and detailed chemical abundances. There are several methods that can be applied for temperature estimation. If the radius and absolute luminosity are known for a star, then its effective temperature can be directly calculated. The shortcoming of this method is that it can only be applied to nearby stars, and for more distant stars other methods are required. For example, calibrated photometric data can be applied to achieve accurate $T_{\rm eff}$ information (e.g., Alonso et al. 1996; Bessell et al 1998; Ramírez & Meléndez 2005; Masana et al. 2006; Mucciarelli et al. 2021), though reliable color excess values are needed for robust results.

Several alternative methods that have been used for decades in stellar $T_{\rm eff}$ determinations are based on high-resolution spectra. Since stellar absorption lines are not affected by interstellar extinction (or reddening), $T_{\rm eff}$ values determined from spectroscopic methods are insensitive to photometric modeling choices, in particular to assumed extinction/reddening parameters. A popular technique requires the absence of any correlation between the abundances obtained from Fe I lines and their excitation potential (EP) values. Such $T_{\rm eff}$ analyses often must take into account possible deviations from

Original content from this work may be used under the terms of the Creative Commons Attribution 4.0 licence. Any further distribution of this work must maintain attribution to the author(s) and the title of the work, journal citation and DOI.

local thermodynamic equilibrium (LTE), and they depend on the use of reliable oscillator strengths and damping coefficients. Balmer lines also become important $T_{\rm eff}$ indicators for stars cooler than 8000 K, because they are almost insensitive to surface gravity in these stars (Heiter & Kupka 2002; Gray 2005). This method involves the comparison of observed Balmer lines with theoretical hydrogen absorption line profiles. Correlations between observed and synthetic spectra (e.g., Cayrel et al. 1991; Prugniel et al. 2011) can also be used for $T_{\rm eff}$ determination.

Line strength ratios of absorption lines have long been used for stellar temperature estimates, especially in spectral classification efforts. Gray & Johanson (1991) first proposed the quantitative application of line depth ratios (LDRs) for accurate $T_{\rm eff}$ derivation from optical region spectroscopy. This technique relies on the central depth ratio of carefully selected absorption lines that have significantly different responses to $T_{\rm eff}$. This method is based on the fact that absorption lines with low and high EP levels respond differently to the temperature changes. Spectral lines with high EP are less responsive to the change in $T_{\rm eff}$ compared to those with low EP. Therefore, the ratio of line depths is a good temperature indicator, which makes the LDR method an attractive option for $T_{\rm eff}$ determination whenever it is applicable. Other parameters, such as metallicity, surface gravity, and micro- and macroturbulence, also affect the line strengths, but here one seeks line pairs where the temperature sensitivity dominates over other atmospheric parameters. Moreover, taking the ratio of line depths comes with the potential advantage of muting dependencies on atmospheric parameters that affect the absorption lines in the same way.

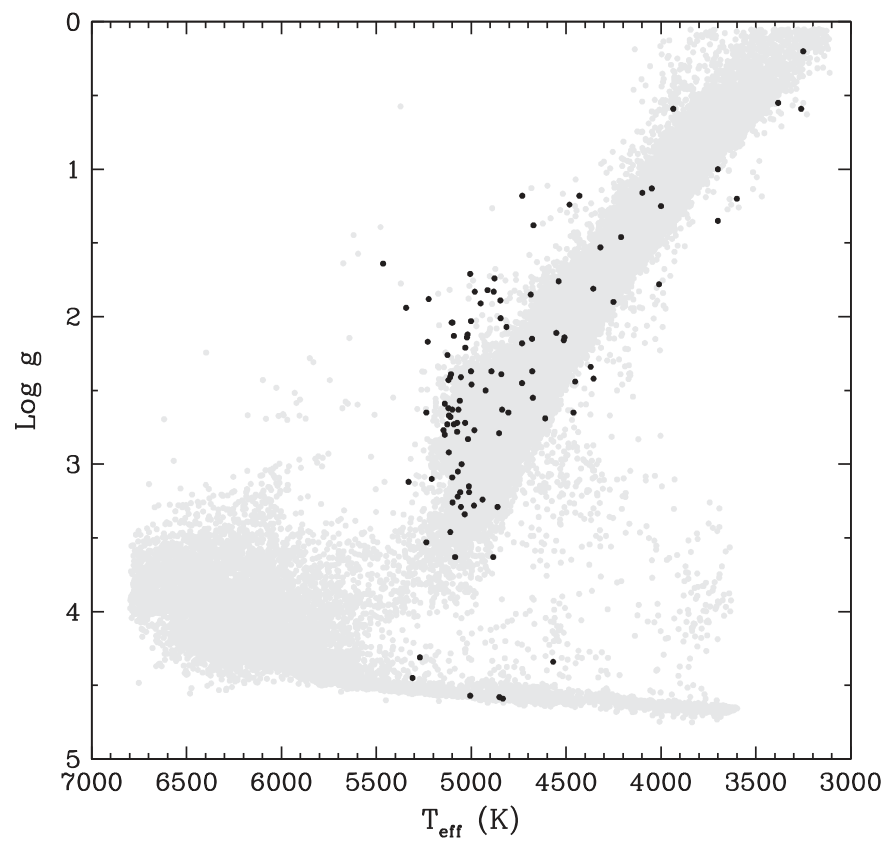


Figure 1. The mean positions of our sample (black dots) on a Kiel diagram. The gray dots represent the data from APOGEE DR17 (Abdurro'uf et al. 2022).

Gray & Johanson (1991) applied the LDR method to just one atomic line pair, $\lambda 6251.8$ and $\lambda 6252.6$, for 49 dwarf stars. Since then, LDR studies have expanded the technique to include other stellar classes and other spectral features. Sasselov & Lester (1990) compared C I and Si I lines near 1 μ m in Cepheids and other cool giants. Gray (1994) increased the 6200 Å region list to 10 line pairs and investigated metallicity corrections for mainsequence stars, and later Gray & Brown (2001) provided LDRs for red giants. A series of studies extending the LDR method in the wavelength region on luminosity class was published by Kovtyukh & Gorlova (2000), Kovtyukh et al. (2003, 2006), and Kovtyukh (2007). LDRs applicable to a 3200-7500 K temperature range for evolved stars were derived by Strassmeier & Schordan (2000). Finally, Biazzo et al. (2007) examined optical LDRs in detail, providing quantitative assessments of luminosity/gravity effects and their influence on the rotational line broadening of various LDR ratios.

However, highly reddened objects suffer from significant interstellar dust extinction, often making them inaccessible in the optical region for high-resolution spectroscopic studies. Therefore, to obtain any information from the objects that are positioned, for example, toward the Galactic center or bulge, the only option is to collect data at longer wavelengths, $\lambda \gtrsim 1~\mu m$. High-resolution infrared spectroscopy is the ideal tool for accessing important stellar atmospheric information from heavily obscured regions. Recent studies suggest that reliable atmospheric parameters of stars can be derived from high-resolution infrared spectral data without any help from the optical region (S. Özdemir et al., 2023, in preparation; E. R. Garro et al., 2023, in preparation).

A $T_{\rm eff}$ determination method of increasing importance in near-infrared high-resolution spectroscopy involves LDRs.

Table 1
Atmospheric Parameters of Stellar Sample

Star	T _{eff} (K)	log g	[M/H]	(km s^{-1})	Reference #a
HIP 80704	3250	0.20	0.07	2.70	1
HIP 69038	3261	0.59	-0.02	2.00	2
HIP 92791	3382	0.55	-0.06	2.30	3
HIP 113881	3600	1.20	-0.11	2.00	1
HIP 50801	3700	1.35	0.00	2.01	4
HIP 67070	3700	1.00	-0.15	2.40	5
HIP 77272	3935	0.59	-0.75	1.66	6
HIP 26386	4000	1.25	-0.55	1.10	7
HIP 102635	4010	1.78	-0.23	2.30	8
HIP 3083	4048	1.13	0.10	2.10	3

Notes.

^a Reference numbers: (1) Smith & Lambert (1985), (2) Koleva & Vazdekis (2012), (3) Prugniel et al. (2011), (4) Mallik (1998), (5) Smith & Lambert (1990), (6) Afşar et al. (2018), (7) Pakhomov (2013), (8) McWilliam (1990), (9) Luck & Challener (1995), (10) Luck (2014), (11) Jönsson et al. (2017), (12) Lyubimkov et al. (2010), (13) Feuillet et al. (2016), (14) Delgado Mena et al. (2017), (15) Hekker & Meléndez (2007), (16) Ramírez et al. (2013), (17) Maldonado et al. (2013), (18) da Silva et al. (2015), (19) Jones et al. (2011), (20) Jofré et al. (2014), (21) Takeda et al. (2008), (22) Luck (2017), (23) Jofré et al. (2015), (24) Tabernero et al. (2012), (25) Takeda et al. (2005), and (26) this study.

(This table is available in its entirety in machine-readable form.)

Recently, Fukue et al. (2015) applied the LDR method to the H-band (1.4 – 1.8 μ m) spectral region for the first time in order to measure more robust effective temperatures of highly reddened stars. They obtained high-resolution (R=20,000)

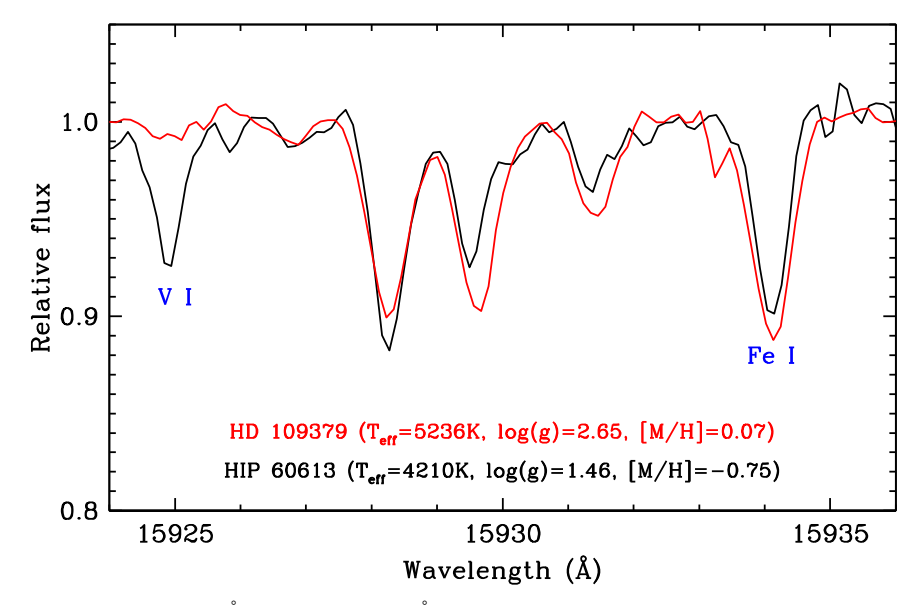


Figure 2. Temperature sensitivity of V I (15924.8 Å) and Fe I (15934.0 Å) absorption lines in HD 109379 ($T_{\rm eff} = 5326$ K) and HIP 60613 ($T_{\rm eff} = 4210$ K).

spectra of 10 well-known G and K giants/supergiants (4000 < $T_{\rm eff}$ (K) < 6000) with the Subaru Infrared Camera and Spectrograph. They found nine LDR pairs of absorption lines and determined $T_{\rm eff}$ values of these stars with an accuracy of ~60 K. Later, Taniguchi et al. (2018) found 81 LDR- $T_{\rm eff}$ relations using the YJ-band (0.90–1.35 μ m) spectra (R = 28,000) of nine giant stars from G to M type (3700 < $T_{\rm eff}$ (K) < 5400), obtained with the WINERED spectrograph attached to the 1.3 m Araki Telescope.

Recently, Jian et al. (2019) have investigated the effects of metallicity and element abundances on line depths from 11 LDR pairs (seven from Fukue et al. 2015) using the *H*-band spectra (R = 22,500) of thousands of giant stars from the Apache Point Observatory Galactic Evolution Experiment (APOGEE) database (Majewski et al. 2017). Their incorporation of abundance-related terms into the LDR– $T_{\rm eff}$ relations resulted in about 30–90 K scatter in the temperature determination for stars of 3700 < $T_{\rm eff}$ (K) < 5000 and $-0.7 < {\rm [Fe/H]} < +0.4$ dex. López-Valdivia et al. (2019) used the line depths of Fe I and Al I absorption lines and molecular OH lines to determine the temperature of 254 K and M dwarfs from the high-resolution *H*-band spectra obtained with the Immersion Grating Infrared Spectrograph (IGRINS; Yuk et al. 2010; Park et al. 2014).

In this work, we extend LDR studies to a wider wavelength range and investigate the LDR– $T_{\rm eff}$ relations in both the H and K bands, using the high-resolution ($R \simeq 45,000$) spectra of 110 stars obtained with IGRINS. To the best of our knowledge, this is the first study in the literature to use high-resolution K-band spectra for LDR analyses.

2. Observations and Stellar Sample

High-resolution ($R \simeq 45,000$), high signal-to-noise ratio (S/N > 100) spectral data of 110 stars were obtained with IGRINS on the 2.7 m Harlan J. Smith Telescope (McDonald Observatory, Texas) and the 4.3 m Lowell Discovery Telescope (Lowell Observatory, Arizona) between the years of 2014 and 2018. The data were reduced using the IGRINS pipeline package version 2.2 (Lee & Gullikson 2016). IGRINS covers the H and K bands (1.48–2.48 μ m) simultaneously, with a small gap of about 100 Å

Table 2
Atomic Lines Used for LDR Pairs

Species	Wavelength	EP	log gf
•	(Å)	(eV)	2 4
VI	15924.822	2.136	-1.200
Fe I	15934.020	6.310	-0.430
Ti I	16635.160	2.350	-1.582
Fe I	16661.390	6.340	-0.070
Ni I	16673.710	6.040	0.100
Co I	16757.640	3.410	-1.310
Ti I	17376.577	4.489	0.747
Fe I	17420.880	3.882	-2.880
Fe I	17433.635	6.411	0.030
Si I	20917.151	6.727	0.575
Si I	20926.149	6.727	-1.074
Fe I	20991.037	4.143	-2.684
Si I	21779.660	6.718	0.420
Ti I	21782.940	1.749	-1.160
Si I	21819.671	6.721	0.170
Si I	21879.324	6.721	0.410
Fe I	21894.996	6.144	-0.360
Ti I	21897.370	1.739	-1.450
Ti I	22004.500	1.730	-1.910
Sc I	22051.985	1.448	-0.840
Na I	22056.400	3.191	0.290
Si I	22062.710	6.727	0.540
Sc I	22065.306	1.439	-0.830
Fe I	22079.852	5.849	-1.400
Na I	22083.662	3.191	-0.013
Ti I	22211.238	1.734	-1.780
Ti I	22232.858	1.739	-1.690
Fe I	22257.107	5.064	-0.710
Fe I	22260.179	5.086	-0.941
Ti I	22274.027	1.749	-1.790
Ti I	22310.617	1.733	-2.071
Ti I	22443.925	1.739	-2.370

between bands. Details of the data reduction process can be found in, e.g., Afşar et al. (2016) and Park et al. (2018).

About 70% of our sample (Table 1) consists of red horizontal-branch stars (also known as secondary red clump

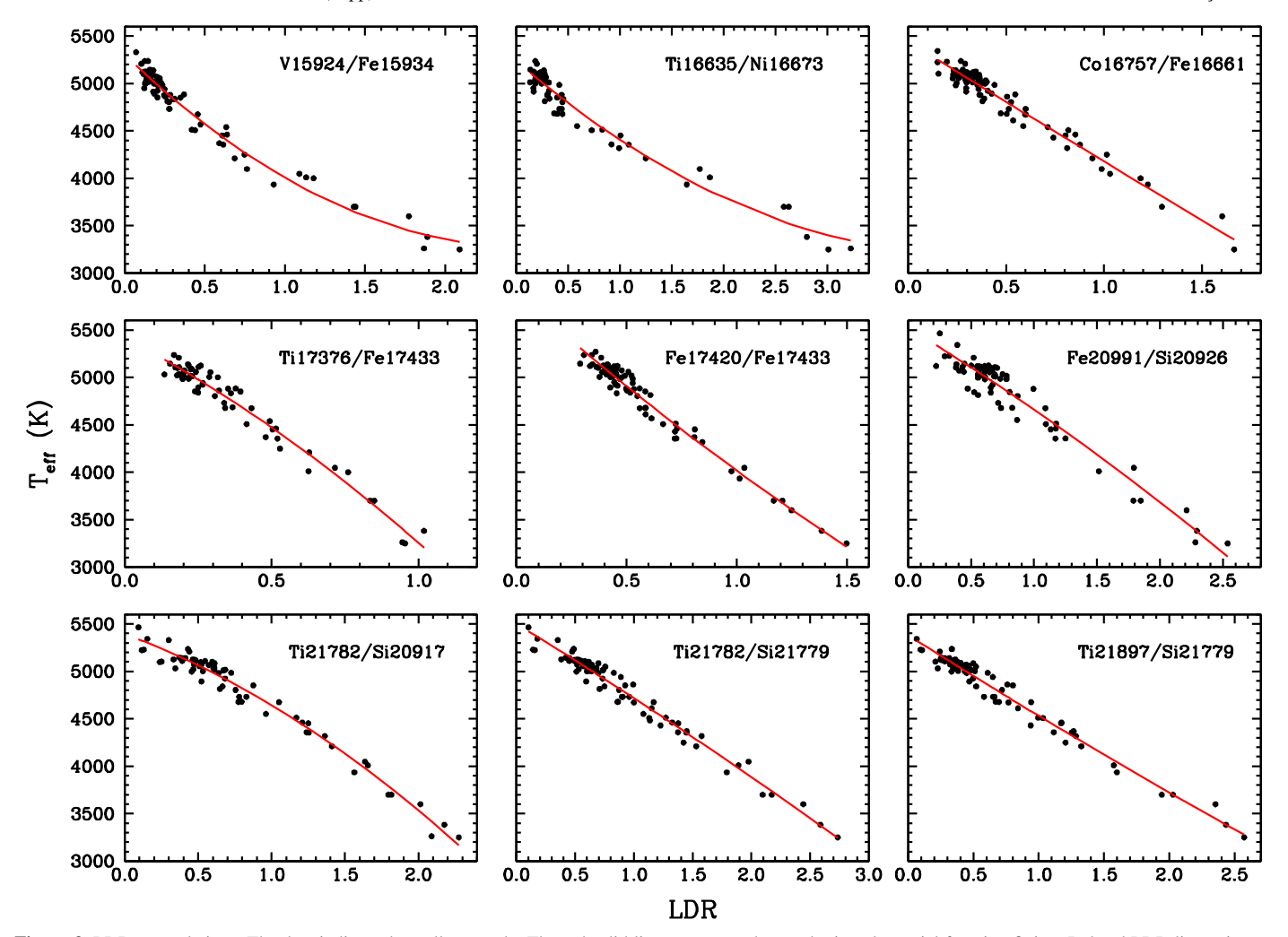


Figure 3. LDR- $T_{\rm eff}$ relations. The dots indicate the stellar sample. The red solid lines represent the quadratic polynomial function fitting. Related LDR line pairs are given in the upper right corners of each panel.

stars) listed in Afşar et al. (2018). The rest of the sample was selected from the IGRINS Spectral Library (Park et al. 2018), mainly to expand the temperature range of our sample, but the selection of these low-temperature stars also extended the surface gravity edges from about 0.2 up to 4.6. Figure 1 shows a Kiel diagram containing the positions of our sample (black dots) along with the stars from APOGEE data release (DR) 17 (gray dots; Abdurro'uf et al. 2022). The Afşar et al. (2018) sample was assembled to investigate the properties of G-K evolved stars warmer than the red giant clump. This accounts for the appearance of stars in Figure 1 with $T_{\rm eff} \sim 5000 \, \rm K$ and $\log g \sim 2$ that lie apart from most of the APOGEE sample. The APOGEE DR17 data used for this diagram contain about 47,000 stars with S/N > 400. The crossmatch of our sample with the APOGEE DR17 data yielded only 11 stars in common. Overall, the stars in our study have temperature, $\log g$, and metallicity ranges of $3200 < T_{\rm eff}$ (K) $< 5500, 0.20 \le$ log g < 4.6, and -1.5 < [M/H] < 0.5, as listed in Table 1.

3. Spectral Line Identification

The LDR method is fundamentally based on the depth ratio of metallic absorption lines with different EP values. As is well known (e.g., Gray & Johanson 1991; Kovtyukh et al. 2003; Fukue et al. 2015, and references therein), lines with low EP are

more responsive to changes in temperature than the ones with high EP. Therefore, different line pairs with low and high EP values are needed to establish the LDR– $T_{\rm eff}$ relations. To find the useful LDR line pairs, we first carried out an atomic line identification process. We carefully examined the whole spectral region by segregating it into wavelength intervals of 10 Å to 50 Å. For each small interval, we generated a synthetic spectrum using the LTE line analysis and synthetic spectrum code MOOG (Sneden 1973). The process of atomic line identification was performed on the spectra of three stars from Afşar et al. (2018) that have high S/N and well represent the temperature range of our entire sample: HIP 64378 ($T_{\rm eff} = 4357$ K), HIP 62653 ($T_{\rm eff} = 4804$ K), and HIP 54048 ($T_{\rm eff} = 5099$ K).

During this process, we made use of the following atomic line sources: NIST (Kramida et al. 2021); VALD3 (Ryabchikova et al. 2015); ATOMIC LINE LIST v2.05b21 (Van Hoof 2018); and papers based on laboratory and stellar spectra (Meléndez & Barbuy 1999; Shetrone et al. 2015). We identified the lines with the simultaneous use of synthetic and observed spectra displayed with the IRAF⁶ splot task. The line

⁵ Available at http://www.as.utexas.edu/~chris/moog.html.

⁶ IRAF is distributed by the National Optical Astronomy Observatory, which is operated by the Association of Universities for Research in Astronomy (AURA) under cooperative agreement with the National Science Foundation.

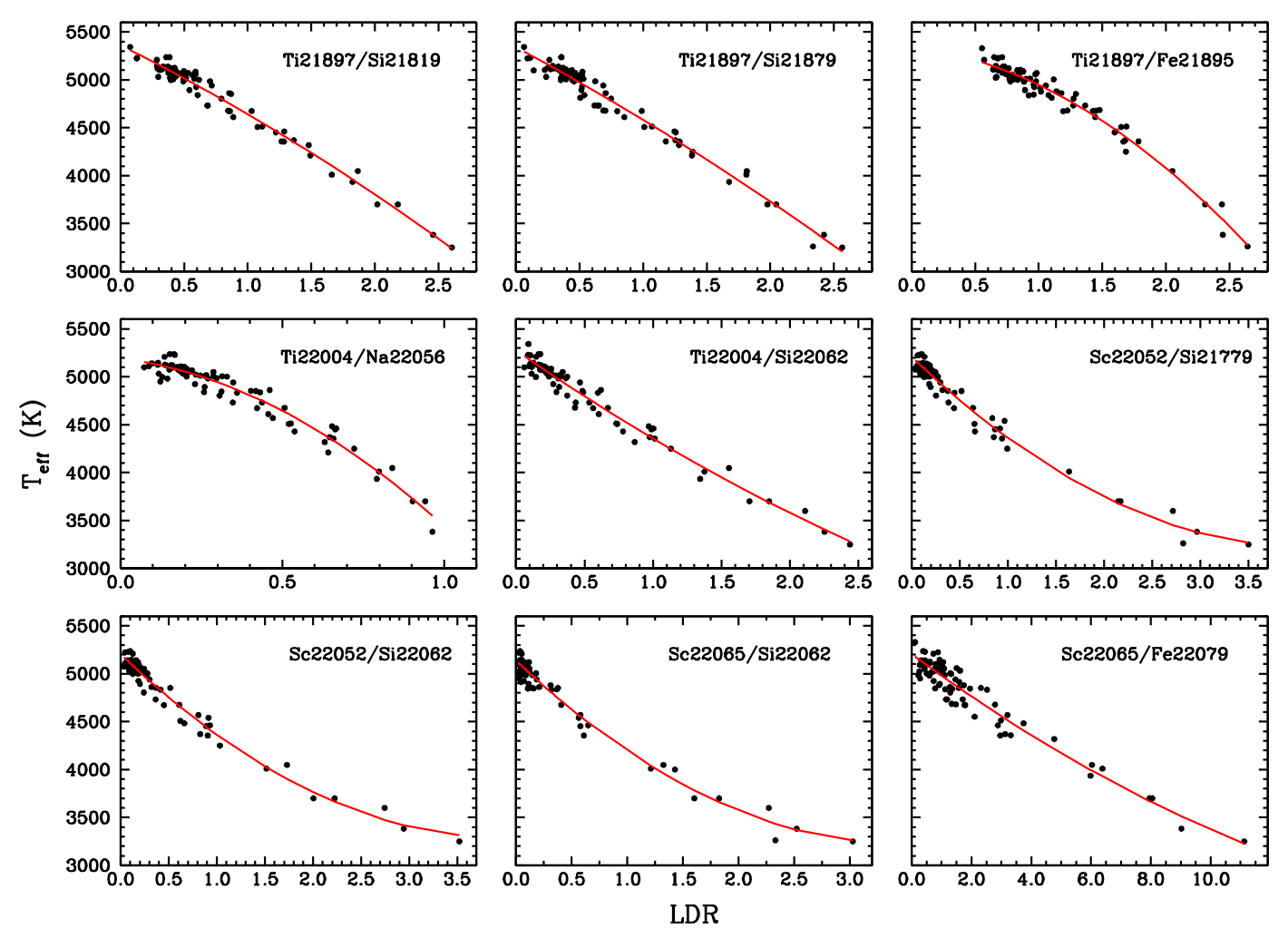


Figure 4. The same as Figure 3.

lists needed for synthetic spectra were generated with the Linemake tool (Placco et al. 2021), which includes atomic lines mainly from Kurucz (2011, 2018) and also contains line transition data from Den Hartog et al. (2021, and references therein). This process led us to identify about 2500 atomic lines in both the H and K bands.

4. Finding LDR Line Pairs and LDR- $T_{\rm eff}$ Relations

After identifying the atomic lines for the complete spectral region, we listed the elements according to their low and high EP values. After the careful selection of plausible atomic absorption lines by eliminating other atomic and molecular contamination as much as possible, we found about 50 potential line pairs. To obtain useful LDR– $T_{\rm eff}$ relations, we first measured their central line depths by applying a Gaussian fitting function using the IRAF splot task. We first selected an initial set of approximately 20 stars from Table 1 that represent the overall temperature range of our sample. Then we measured the ratio of the line depths and plotted against spectral $T_{\rm eff}$ values for this small sample. After examining the LDR– $T_{\rm eff}$ calibrations, we found 32 atomic lines (Table 2) to be useful for LDR method application. Matching these atomic lines yielded 26 LDR line pairs (Table 3) with significant LDR– $T_{\rm eff}$

relationships. An example line pair of V I (15924.8 Å) and Fe I (15934.0 Å) is given in Figure 2. It is important to select LDR line pairs at wavelengths as close as possible to minimize the errors that might originate from the continuum level setting (e.g., Figure 4 in Biazzo et al. 2007 and Table 5 in Taniguchi et al. 2018). Unfortunately, there are not many absorption lines that can satisfy this constraint in the H- and K-band wavelength region. Therefore, we were forced to pair lines that are not in the same spectral order and to use the same absorption line in different line pairs.

Finally, we carried out the line depth measurements for the overall sample (Table 1). The ratios of the line pairs (low EP/ high EP) were plotted against the spectral $T_{\rm eff}$ values that were collected from various literature sources (the reference list for the spectral $T_{\rm eff}$ values is given in Table 1). It should be noted here that not all the line depths could be measured for every star. For example, some weak atomic lines could not be detected in metal-poor stars ([M/H] < -1). A couple of stars turned out to be spectroscopic binaries that had not been previously noticed. Additionally, some data problems, such as low S/Ns or problematic telluric line removal, resulted in the elimination of some of the line pairs in a few stars. To characterize the LDR- $T_{\rm eff}$ relationships, we used quadratic polynomial functions $(T_{\text{eff}} = ax^2 + bx + c, \text{ where } x \text{ is a})$ particular LDR) to best represent the distribution of the data points in all of the calibrations. To increase the sensitivity of

https://github.com/vmplacco/linemake

Table 3 LDR Pairs and Polynomial Coefficients for LDR– T_{eff} Relations^a

#	Species	Wavelength (Å)	Low EP (eV)	Species	Wavelength (Å)	High EP (eV)	а	b	С
1	VI	15924.822	2.136	Fe I	15934.020	6.310	325.80	-1623.00	5302.2
2	Ti I	16635.160	2.350	Ni I	16673.710	6.040	109.47	-940.02	5237.0
3	Co I	16757.640	3.410	Fe I	16661.390	6.340	12.43	-1273.00	5440.5
4	Ti I	17376.577	4.489	Fe I	17433.635	6.411	-544.70	-1615.90	5417.1
5	Fe I	17420.880	3.882	Fe I	17433.635	6.411	172.50	-2039.50	5884.8
6	Fe I	20991.037	4.143	Si I	20926.149	6.727	-57.92	-802.41	5521.3
7	Ti I	21782.940	1.749	Si I	20917.151	6.727	-179.63	-570.72	5394.5
8	Ti I	21782.940	1.749	Si I	21779.660	6.718	-24.00	-759.71	5501.4
9	Ti I	21897.370	1.739	Si I	21779.660	6.718	21.27	-871.57	5382.1
10	Ti I	21897.370	1.739	Si I	21819.671	6.721	-58.17	-661.10	5360.5
11	Ti I	21897.370	1.739	Si I	21879.324	6.721	-45.67	-714.48	5340.6
12	Ti I	21897.370	1.739	Fe I	21894.996	6.144	-239.59	-155.53	5341.8
13	Ti I	22004.500	1.730	Na I	22056.400	3.191	-1311.80	-442.95	5193.8
14	Ti I	22004.500	1.730	Si I	22062.710	6.727	71.95	-991.17	5274.7
15	Sc I	22051.985	1.448	Si I	21779.660	6.718	117.55	-966.01	5208.8
16	Sc I	22051.985	1.448	Si I	22062.710	6.727	120.91	-962.31	5204.5
17	Sc I	22065.306	1.439	Si I	22062.710	6.727	158.02	-1098.40	5135.6
18	Sc I	22065.306	1.439	Fe I	22079.852	5.849	4.70	-230.17	5205.1
19	Sc I	22065.306	1.439	Na I	22083.662	3.191	429.44	-1988.20	5182.1
20	Ti I	22211.238	1.734	Fe I	22257.107	5.064	-285.66	-581.50	5260.3
21	Ti I	22211.238	1.734	Fe I	22260.179	5.086	-164.53	-694.44	5323.4
22	Ti I	22232.858	1.739	Fe I	22257.107	5.064	-341.30	-439.41	5248.7
23	Ti I	22232.858	1.739	Fe I	22260.179	5.086	-135.50	-707.92	5374.1
24	Ti I	22274.027	1.749	Fe I	22257.107	5.064	-405.20	-428.16	5225.9
25	Ti I	22310.617	1.733	Fe I	22257.107	5.064	-42.72	-1135.70	5262.3
26	Ti I	22443.925	1.739	Fe I	22260.179	5.086	219.42	-1518.80	5259.2

Notes

Star	T _{eff} (K)	T _{LDR} (K)	T _{eff} (Gaia) (K)	$\frac{T_{\rm eff}(J-K)}{({\rm K})}$
HIP 80704	3250	3279		3555
HIP 69038	3261	3383		3451
HIP 92791	3382	3408		3610
HIP 113881	3600	3480		3982
HIP 67070	3700	3694	3851	3711
HIP 50801	3700	3705		4084
HIP 77272	3935	4008	4065	3727
HIP 26386	4000	3866	4250	3695
HIP 102635	4010	4006	4061	4014
HIP 3083	4048	3939	4017	3802

(This table is available in its entirety in machine-readable form.)

the calibrations, we ran multiple iterations to identify and eliminate aberrant data points. The method that we used for iterations requires the difference between the actual (spectral $T_{\rm eff}$ values; Table 1) and calculated LDR temperatures ($\Delta T_{\rm eff} = T_{\rm eff} - T_{\rm LDR}$) to be below the 2σ level of the $\Delta T_{\rm eff}$ distribution. We ran the iterations until all the $\Delta T_{\rm eff}$ values satisfied this requirement—in other words, all the outlier data with values higher than the 2σ level were removed through these iterations—which, in turn, led us to use about 70–90 stars for the final LDR- $T_{\rm eff}$ calibrations, depending on the line pairs studied. All of the final LDR- $T_{\rm eff}$ relationships are plotted in

Figures 3, 4, and 5, and the quadratic polynomial coefficients are provided in Table 3.

4.1. Uncertainties in T_{eff} Determination

In Table 4, we list the mean LDR temperatures $(\overline{T_{LDR}})$ for the entire sample, except for HIP 79248, where we could not measure the LDRs from any of the line pairs listed in Table 3. The $\overline{T_{LDR}}$ temperatures were obtained by taking the simple average of the individual LDR temperatures calculated from the quadratic polynomial functions given in Table 3. The standard errors (SE = σ/\sqrt{n}) and σ values for the LDR temperatures of each star range between $\pm 4 \lesssim$ SE $\lesssim \pm 60$ and $20 \lesssim \sigma \lesssim 150$. The means of the standard errors (\overline{SE}) and standard deviations ($\overline{\sigma}$) were found as $\overline{SE} = \pm 15$ K and $\overline{\sigma} = 59$ K, showing the overall internal uncertainty level of the $\overline{T_{LDR}}$ temperatures obtained from each line pair.

We crossmatched our sample with Gaia DR3 (Gaia Collaboration et al. 2016, 2022), finding Gaia spectral temperatures (Recio-Blanco et al. 2022) for 94 of our sample stars. We also calculated photometric temperatures for 107 stars with available Two Micron All Sky Survey (2MASS) J and K magnitudes (Skrutskie et al. 2006) using the relations provided by González Hernández & Bonifacio (2009). The spectral temperatures gathered from the literature ($T_{\rm eff}$; see also Table 1) and the $T_{\rm eff}$ (Gaia) spectral and $T_{\rm eff}$ (J-K) photometric temperatures are also listed in Table 4 for comparison. The uncertainty level of the temperatures resulting from the application of our LDR method was estimated by comparing the $T_{\rm LDR}$ temperatures with the ones gathered from the

^a All LDR- T_{eff} relations are represented with quadratic polynomials ($T_{\text{eff}} = ax^2 + bx + c$), in which x is the LDR value.

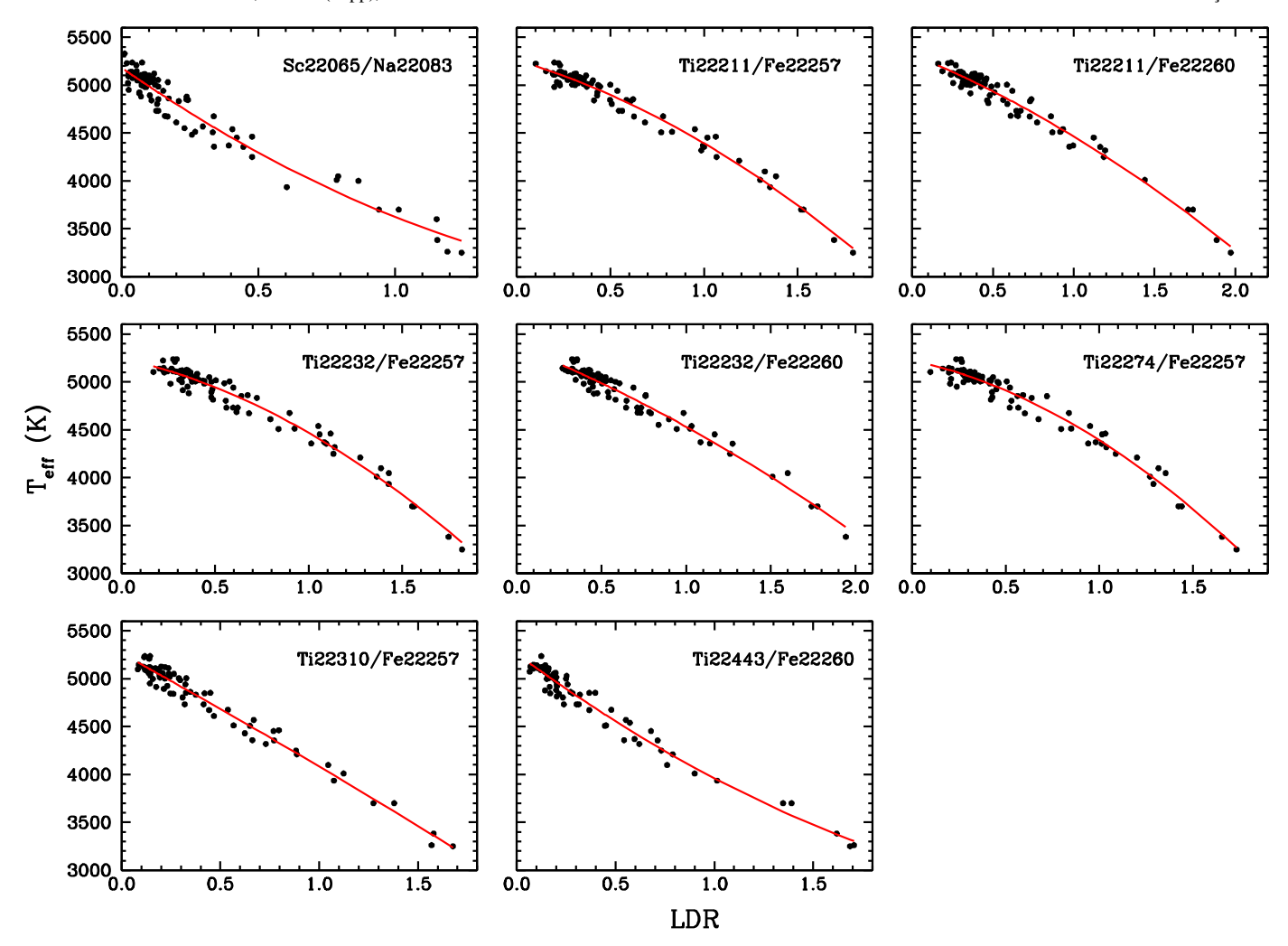


Figure 5. The same as Figure 3.

literature, $T_{\rm eff}$. The standard deviation of the $(T_{\rm eff}-\overline{T_{\rm LDR}})$ differences yielded the uncertainty level of our method as $\sigma(T_{\rm eff}-\overline{T_{\rm LDR}})\simeq 70~{\rm K}$.

We also compared our results with the spectral Gaia temperatures (Recio-Blanco et al. 2022) and obtained $\sigma(T_{\rm eff}({\rm Gaia}) - \overline{T_{\rm LDR}}) \simeq 145$ K. A plot that compares the spectral $T_{\rm eff}$ values with the $T_{\rm LDR}$ and $T_{\rm eff}({\rm Gaia})$ temperatures is given in Figure 6. The good agreement between the temperatures is noteworthy.

Although obtained using two different measurement methods, we also compared our LDR temperatures with the $T_{\rm eff}(J-K)$ photometric temperatures and $\sigma(T_{\rm eff}(J-K)-\overline{T_{\rm LDR}}) \simeq 340$ K. This substantial deviation between the temperatures mainly originates from the J- and Kmagnitude uncertainties reported in the 2MASS catalog. For example, an uncertainty of about 0.25 mag in J magnitude results in an uncertainty level of about 1000 K in the $T_{\rm eff}(J-K)$ temperature. When we narrow down the 2MASS sample by limiting the uncertainties in both the J and Kmagnitudes by taking into account only the stars with J- and Kmagnitude uncertainties of lower than 0.2 mag, the crossmatch of our sample yields only 58 stars in common, which, in turn, gives $\sigma(T_{\rm eff}(J-K)-\overline{T_{\rm LDR}}) \simeq 175$ K.

Unfortunately, there are not many G-K standard stars that have been observed with IGRINS, which makes it difficult to test the accuracy level of our LDR- $T_{\rm eff}$ relations for stars that

are outside our current sample. The only prominent star for which we have IGRINS spectral data is Arcturus. Running all the LDR- $T_{\rm eff}$ relations on Arcturus, we obtained $\overline{T_{\rm LDR}}=4263\pm14$ K ($\sigma=62$ K) from 19 line pairs, in excellent agreement with the temperature reported by, e.g., Ramírez & Allende Prieto (2011; $T_{\rm eff}=4286\pm30$ K) and with the literature in general. The LDR- $T_{\rm eff}$ relations from which we did not receive reliable temperature information for Arcturus were mostly the ones with Sc involved (Table 3), and two additional line pairs in the K band (Fe20991/Si20926, Ti21897/Fe21894) also could not be used. In Section 5, we will discuss these line pairs in more detail.

We also tested the LDR– $T_{\rm eff}$ relations on two open cluster members, NGC 6940 MMU 105 and NCG 752 MMU 77, which were previously observed with IGRINS by our group (Böcek Topcu et al. 2016, 2019, 2020). For NGC 6940 MMU 105, we found $\overline{T_{\rm LDR}}=4813\pm10$ K ($\sigma=41$ K) from 18 line pairs, which is in good agreement with $T_{\rm eff}=4765\pm100$ K from Böcek Topcu et al. (2016). The same few anomalous line pairs that we identified in Arcturus showed a similar behavior in the MMU 105 case. Additionally, we could not measure the depths of two line pairs, Ti17376/Fe17433 and Ti22310/Fe22257, for this star.

For NCG 752 MMU 77, we calculated the LDR temperatures from 21 line pairs. Taking an average of the individual $T_{\rm LDR}$ values yielded $\overline{T_{\rm LDR}} = 4869 \pm 12$ K ($\sigma = 60$ K), which is

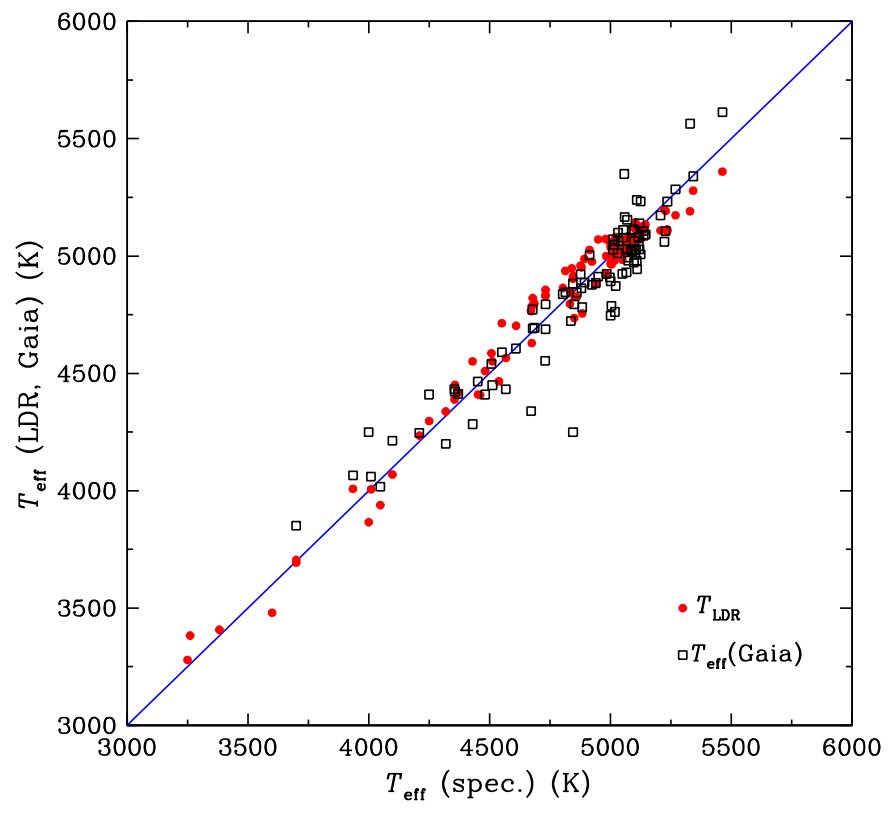


Figure 6. Comparison of the spectral $T_{\rm eff}$ values reported in the literature with the $\overline{T_{\rm LDR}}$ (red dots) and spectral $T_{\rm eff}$ (Gaia) (open squares) temperatures (Recio-Blanco et al. 2022). The blue line represents the perfect fit (x = y).

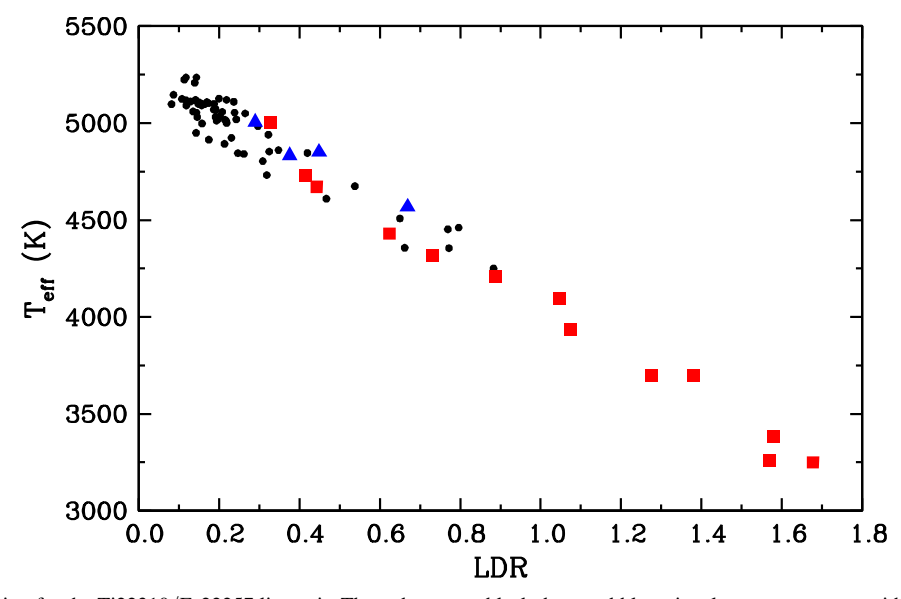


Figure 7. The LDR- $T_{\rm eff}$ relation for the Ti22310/Fe22257 line pair. The red squares, black dots, and blue triangles represent stars with $0.20 \leqslant \log g \leqslant 1.71, 1.78 \leqslant \log g \leqslant 3.53$, and $4.40 < \log g < 4.60$, respectively.

in quite good agreement with $T_{\rm eff} = 4874 \pm 100$ K from Böcek Topcu et al. (2015).

Setting the continuum level in both the *H*- and *K*-band spectra of especially cool stars is difficult, because they have rich spectra of many complex absorption and molecular features. Despite our effort to select the absorption lines of LDR with no obvious blending issues, crowded spectral regions in the *H* and *K* bands are still inevitable in cool stars. Therefore, continuum placement is not perfectly defined for

every LDR pair. To be able to minimize the temperature uncertainties caused by the continuum placement between the central line depth measurements, we preferred to place the continuum locally during the Gaussian line fitting to the related absorption lines. To estimate the temperature uncertainties arising from the continuum level placement, we used a small set of stars that well represent the temperature distribution of our overall sample: HD 148783, HD 119667, HIP 97599, HIP 27091, and HIP 33578 (Table 1). We applied a simple

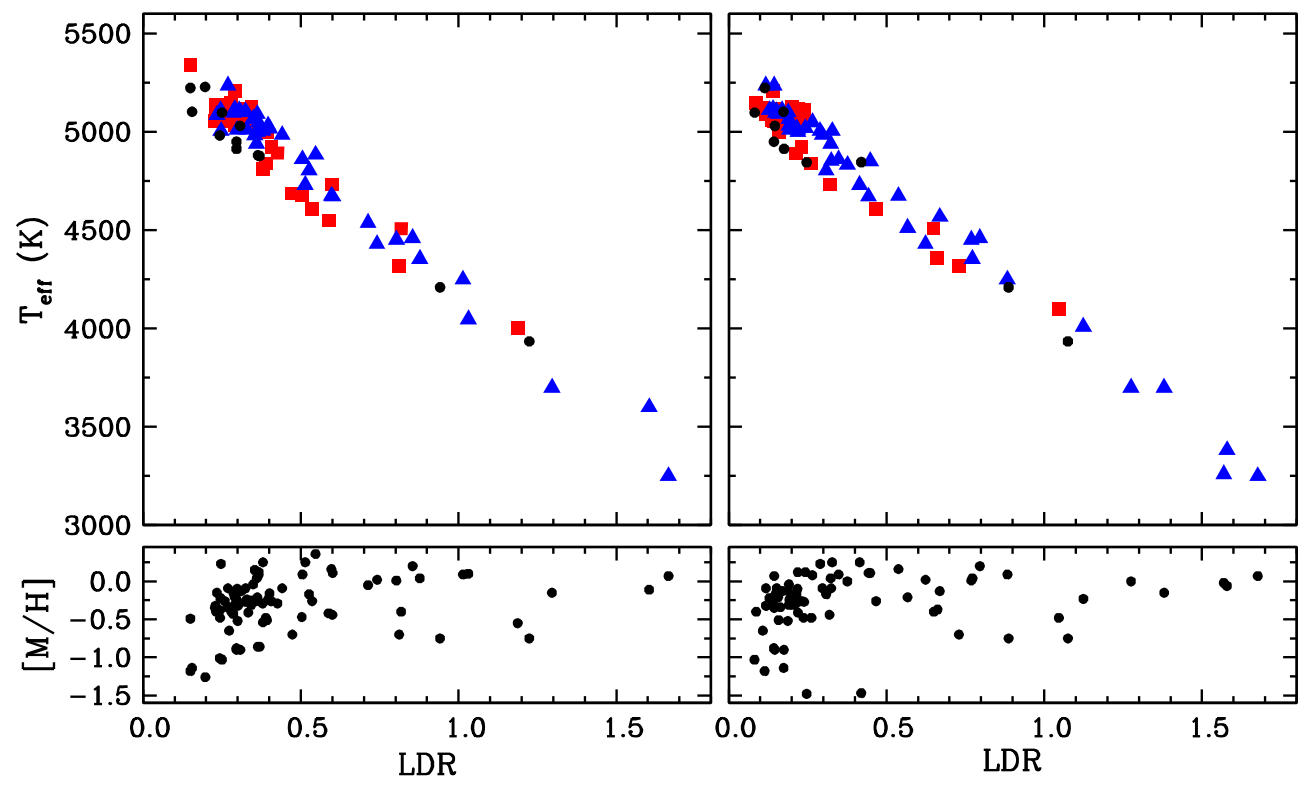


Figure 8. An example of the metallicity effect on LDR- $T_{\rm eff}$ relations for both the H and K bands: Co16757/Fe16661 (left) and Ti22310/Fe22257 (right). In the upper panels, the stars with [M/H] < -0.75, $-0.75 \le [M/H] \le -0.25$, and $-0.25 \le [M/H] < 0.4$ are colored in black (dots), red (squares), and blue (triangles), respectively. The lower panels show the LDR-metallicity distribution for Co16757/Fe16661 (left) and Ti22310/Fe22257 (right).

approximation and measured the depths of the lines six times for the same star by varying the local continuum to form a set of 30 LDR measurements for the individual line pairs in both the H and K bands. The average temperature uncertainties that emerge from the LDRs obtained for both regions are 39 ± 5 K ($\sigma = 29$ K) and 23 ± 4 K ($\sigma = 22$ K) for the H and K bands, respectively.

5. Discussion

5.1. The Luminosity Dependency of LDRs

The use of LDRs of luminosity-sensitive and nonsensitive absorption lines for luminosity classification dates back many decades (e.g., Wright & Jacobson 1965). The effect of luminosity, in other words surface gravity, on LDRs has been discussed in several studies, such as Gray & Brown (2001), Biazzo et al. (2007), and Jian et al. (2020). The latter paper investigated the gravity effect on LDRs obtained from the *YJ*-band spectra of a group of stars with a $T_{\rm eff}$ range of 3500–8000 K, including dwarfs, giants, and supergiants. They found that some of the line pairs they use for LDR– $T_{\rm eff}$ calibrations show systematic offsets between the three luminosity groups. Their investigation led to a conclusion that the depths of some neutral lines (e.g., Si I at $\lambda\lambda$ 10371) in their LDR pairs are sensitive to log g, while others not (e.g., Ca I at $\lambda\lambda$ 10343).

Recently, Matsunaga et al. (2021) proposed a method that uses LDRs as indicators of the $T_{\rm eff}$ and $\log g$. They found empirical relations between $T_{\rm eff}$, $\log g$, and the LDRs, which they derived using selected line pairs of Fe I–Fe II and Ca I –Ca II lines from the YJ-band spectra of a sample of stars from dwarfs to supergiants. From this method, they reported

precision levels of 50 K and 0.2 dex for the $T_{\rm eff}$ and $\log g$ determinations, respectively.

In general, the ionized species are more sensitive to changes in gravity than the neutral ones in cool stars, though strong lines of neutral species, such as the Mg I b triplet near 5170 Å (e.g., Gray 2005), are known to be sensitive to surface gravity changes, mainly due to the pressure sensitivity of the damping constant. Our sample has stars with surface gravities between $0.20 \le \log g < 4.6$, but it mainly contains giant stars with only a few main-sequence and supergiant stars. The cool end of our sample contains fewer stars with $\log g < 1.75$, leaving not enough room to statistically investigate the LDR- $T_{\rm eff}$ relations for supergiants. On the other hand, having mostly weak lines as LDR pairs, our investigation of the $\log g$ effect on the LDR- $T_{\rm eff}$ calibrations (e.g., Figure 7) showed no systematic offsets for different luminosity groups, allowing us to use the LDR- $T_{\rm eff}$ relations as listed in Table 3 without any apparent need for $\log g$ correction on LDRs.

5.2. The Metallicity Effect on LDRs

The metallicity dependence of LDRs has been previously discussed in several studies. Gray & Brown (2001) noted the effects of metallicity, absolute magnitude, and temperature on spectral lines. To improve the precision of the LDR-temperature calibrations in their work, they applied corrections for metallicity variations to the LDRs. The H-band studies of Fukue et al. (2015) and Jian et al. (2019) also investigated the effects of metallicity and abundance ratios on LDR- $T_{\rm eff}$ relations. The Jian et al. (2019) analysis is especially useful, as they used a large number of H-band spectra (3700 $< T_{\rm eff} < 5000$ K) from the APOGEE survey with a metallicity range of $-0.7 < [{\rm Fe}/{\rm H}] < 0.4$ dex. They interpreted the saturations

on abundance ratios to explain the metallicity effect on the LDRs. Our sample has a metallicity range of $-1.5 < [\mathrm{M/H}] < 0.5$. Investigating the metallicity range on LDRs, we found no clear relation between LDRs and the metallicities. An example plot that searches for the effect of [M/H] on LDR- T_{eff} relations is given in Figure 8. However, our stellar sample of 110 stars is too small to explore all of the possible parameter dependencies of these newly defined LDR relationships. The expansion of our sample size will be taken up in a future LDR calibration study.

5.3. Line Pairs with Blended Features

For cool stars, the near-infrared, especially the K-band spectral region, is dominated by many molecular lines, making it difficult to find unblended atomic lines. We noticed that some of the LDR- $T_{\rm eff}$ calibrations listed in Table 3 tend to give temperatures about 100–200 K higher than the literature $T_{\rm eff}$ values (Table 1) when applied to stars that are not included in our sample (Section 4.1): Arcturus, NGC 6940 MMU 105, and NCG 752 MMU 77. These LDR- $T_{\rm eff}$ calibrations are usually the ones that have atomic lines paired with Sc I 22052 Å and 22065 Å lines (also numbered as 15, 16, 17, 18, and 19 in Table 3). Closer examination of the scandium lines indicated that the Sc I 22052 A line was blended with a Si I line (22051.93 Å). Although the λ 22065 Sc I line is unblended, a nearby CO feature becomes more intrusive at temperatures ≤4800 K. Two additional line pairs, Fe I 20991/Si I 20926 and $\stackrel{\sim}{\text{Ti}}$ I 21897/Fe I 21895, were also found to be affected by the contribution of CO features that seem to become more potent especially for stars with $T_{\rm eff} \lesssim 4800$ K. These LDR line pairs should be applied with caution.

6. Summary and Conclusion

In this study, we have applied the LDR method to highresolution near-infrared spectra of 110 stars, which were obtained with IGRINS in the H and K bands, simultaneously. To our knowledge, this is the first study that reports the LDR- $T_{\rm eff}$ relations in the K-band spectral region. Our sample covers mostly giant stars, along with several main-sequence stars and supergiants. Performing LDR- $T_{\rm eff}$ calibrations, we found 26 LDR line pairs that are mostly composed of Fe-peak elements (Table 3) and provide temperatures comparable to literature $T_{\rm eff}$ values within an accuracy of about 70 K. The investigation of our LDR-Teff relations for the dependence of the LDRs on $\log g$ and [M/H] resulted in no clear relations. We suggest further investigation of these parameters with a more extensive sample drawn from the Raw and Reduced IGRINS Spectral Archive⁸ (Sawczynec et al. 2022) in a future LDR study.

We thank our referee for helpful comments that improved this paper. Our work has been supported by The Scientific and Technological Research Council of Turkey (TÜBİTAK, project No. 119F076), by the US National Science Foundation grant AST-1616040, and by the University of Texas Rex G. Baker, Jr. Centennial Research Endowment. This work used the Immersion Grating Infrared Spectrometer (IGRINS) that was developed under a collaboration between the University of Texas at Austin and the Korea Astronomy and Space Science

Institute (KASI) with the financial support of the Mt. Cuba Astronomical Foundation, of the US National Science Foundation under grants AST-1229522 and AST-1702267, of the McDonald Observatory of the University of Texas at Austin, of the Korean GMT Project of KASI, and of the Gemini Observatory. This material is based upon work supported by the National Science Foundation under grant No. AST-1908892 to G.M. R.L.V. acknowledges support from CON-ACYT through a postdoctoral fellowship within the program "Estancias Posdoctorales por México." S.Ö. also acknowledges support by the National Science Centre, Poland, project 2019/ 34/E/ST9/00133. This work has made use of data from the European Space Agency (ESA) mission Gaia (https://www. cosmos.esa.int/Gaia), processed by the Gaia Data Processing and Analysis Consortium (DPAC, https://www.cosmos.esa. int/web/Gaia/dpac/consortium). Funding for the DPAC has been provided by national institutions, in particular the institutions participating in the Gaia Multilateral Agreement. This publication makes use of data products from the Two Micron All Sky Survey, which is a joint project of the University of Massachusetts and the Infrared Processing and Analysis Center/California Institute of Technology, funded by the National Aeronautics and Space Administration and the National Science Foundation. This research has made use of the SIMBAD database, operated at CDS, Strasbourg, France.

Software: IRAF (Tody 1993 and references therein), MOOG (Sneden 1973), ATLAS (Kurucz 2011).

ORCID iDs

Melike Afşar https://orcid.org/0000-0002-2516-1949
Zeynep Bozkurt https://orcid.org/0000-0002-4413-4401
Sergen Özdemir https://orcid.org/0000-0003-1500-332X
Christopher Sneden https://orcid.org/0000-0002-3456-5929
Gregory N. Mace https://orcid.org/0000-0001-7875-6391
Daniel T. Jaffe https://orcid.org/0000-0003-3577-3540
Ricardo López-Valdivia https://orcid.org/0000-0002-7795-0018

References

```
Abdurro'uf, Accetta, K., Aerts, C., et al. 2022, ApJS, 259, 35
Afşar, M., Bozkurt, Z., Böcek Topcu, G., et al. 2018, AJ, 155, 240
Afşar, M., Sneden, C., Frebel, A., et al. 2016, ApJ, 819, 103
Alonso, A., Arribas, S., & Martinez-Roger, C. 1996, A&AS, 117, 227
Bessell, M. S., Castelli, F., & Plez, B. 1998, A&A, 333, 231
Biazzo, K., Frasca, A., Catalano, S., & Marilli, E. 2007, AN, 328, 938
Böcek Topcu, G., Afşar, M., Schaeuble, M., & Sneden, C. 2015, MNRAS,
   446, 3562
Böcek Topcu, G., Afşar, M., & Sneden, C. 2016, MNRAS, 463, 580
Böcek Topcu, G., Afşar, M., Sneden, C., et al. 2019, MNRAS, 485, 4625
Böcek Topcu, G., Afşar, M., Sneden, C., et al. 2020, MNRAS, 491, 544
Cayrel, R., Perrin, M. N., Barbuy, B., & Buser, R. 1991, A&A, 247, 108
da Silva, R., Milone, A. d., & Rocha-Pinto, H. J. 2015, A&A, 580, A24
Delgado Mena, E., Tsantaki, M., Adibekyan, V. Z., et al. 2017, A&A,
Den Hartog, E. A., Lawler, J. E., Sneden, C., et al. 2021, ApJS, 255, 27
Feuillet, D. K., Bovy, J., Holtzman, J., et al. 2016, ApJ, 817, 40
Fukue, K., Matsunaga, N., Yamamoto, R., et al. 2015, ApJ, 812, 64
Gaia Collaboration, Prusti, T., de Bruijne, J. H. J., et al. 2016, A
Gaia Collaboration, Vallenari, A., Brown, A. G. A., et al. 2022, arXiv:2208.
   00211
González Hernández, J. I., & Bonifacio, P. 2009, A&A, 497, 497
Grav. D. F. 1994, PASP, 106, 1248
Gray, D. F. 2005, The Observation and Analysis of Stellar Photospheres (3rd
  ed.; Cambridge: Cambridge Univ. Press)
Gray, D. F., & Brown, K. 2001, PASP, 113, 723
Gray, D. F., & Johanson, H. L. 1991, PASP, 103, 439
```

https://igrinscontact.github.io/

Masana, E., Jordi, C., & Ribas, I. 2006, A&A, 450, 735

506, 1031

Matsunaga, N., Jian, M., Taniguchi, D., & Elgueta, S. S. 2021, MNRAS,

```
Heiter, U., Kupka, F., van't Veer-Menneret, C., et al. 2002, A&A, 392, 619
Hekker, S., & Meléndez, J. 2007, A&A, 475, 1003
Jian, M., Matsunaga, N., & Fukue, K. 2019, MNRAS, 485, 1310
Jian, M., Taniguchi, D., Matsunaga, N., et al. 2020, MNRAS, 494, 1724
Jofré, E., Petrucci, R., Saffe, C., et al. 2015, A&A, 574, A50
Jofré, P., Heiter, U., Soubiran, C., et al. 2014, A&A, 564, A133
Jones, M. I., Jenkins, J. S., Rojo, P., & Melo, C. H. F. 2011, A&A, 536, A71
Jönsson, H., Ryde, N., Nordlander, T., et al. 2017, A&A, 598, A100
Koleva, M., & Vazdekis, A. 2012, A&A, 538, A143
Kovtyukh, V. V. 2007, MNRAS, 378, 617
Kovtyukh, V. V., & Gorlova, N. I. 2000, A&A, 358, 587
Kovtyukh, V. V., Soubiran, C., Belik, S. I., & Gorlova, N. I. 2003, A&A,
   411, 559
Kovtyukh, V. V., Soubiran, C., Bienaymé, O., Mishenina, T. V., & Belik, S. I.
   2006, MNRAS, 371, 879
Kramida, A., Ralchenko, Y. R. J., NIST ASD Team, et al. 2021, NIST Atomic
   Spectra Database (version 5.9) (Gaithersburg, MD: National Institute of
   Standards and Technology)
Kurucz, R. L. 2011, CaJPh, 89, 417
Kurucz, R. L. 2018, in ASP Conf. Ser. 515, Workshop on Astrophysical
   Opacities, 47
Lee, J.-J., & Gullikson, K. 2016, Plp: V2.1 Alpha 3, v2.1-alpha.3, Zenodo,
   Zenodo, doi:10.5281/zenodo.56067
López-Valdivia, R., Mace, G. N., Sokal, K. R., et al. 2019, ApJ, 879, 105
Luck, R. E. 2014, AJ, 147, 137
Luck, R. E. 2017, AJ, 153, 21
Luck, R. E., & Challener, S. L. 1995, AJ, 110, 2968
Lyubimkov, L. S., Lambert, D. L., Rostopchin, S. I., Rachkovskaya, T. M., &
   Poklad, D. B. 2010, MNRAS, 402, 1369
Maiewski, S. R., Schiavon, R. P., Frinchaboy, P. M., et al. 2017, AJ, 154, 94
Maldonado, J., Villaver, E., & Eiroa, C. 2013, A&A, 554, A84
Mallik, S. V. 1998, A&A, 338, 623
```

```
McWilliam, A. 1990, ApJS, 74, 1075
Meléndez, J., & Barbuy, B. 1999, ApJS, 124, 527
Mucciarelli, A., Bellazzini, M., & Massari, D. 2021, A&A, 653, A90
Pakhomov, Yu. V. 2013, AstL, 39, 54
Park, C., Jaffe, D. T., Yuk, I.-S., et al. 2014, Proc. SPIE, 9147, 91471D
Park, S., Lee, J.-E., Kang, W., et al. 2018, ApJS, 238, 29
Placco, V. M., Sneden, C., Roederer, I. U., et al. 2021, RNAAS, 5, 92
Prugniel, P., Vauglin, I., & Koleva, M. 2011, A&A, 531, A165
Ramírez, I., & Allende Prieto, C. 2011, ApJ, 743, 135
Ramírez, I., Allende Prieto, C., & Lambert, D. L. 2013, ApJ, 764, 78
Ramírez, I., & Meléndez, J. 2005, ApJ, 626, 465
Recio-Blanco, A., de Laverny, P., Palicio, P. A., et al. 2022, arXiv:2206.05541
Ryabchikova, T., Piskunov, N., Kurucz, R. L., et al. 2015, PhyS, 90, 054005
Sasselov, D. D., & Lester, J. B. 1990, ApJ, 360, 227
Sawczynec, E., Mace, G., Gully-Santiago, M., & Jaffe, D. 2022, BAAS, 54,
  2022n6i203p06
Shetrone, M., Bizyaev, D., Lawler, J. E., et al. 2015, ApJS, 221, 24
Skrutskie, M. F., Cutri, R. M., Stiening, R., et al. 2006, AJ, 131, 1163
Smith, V. V., & Lambert, D. L. 1985, ApJ, 294, 326
Smith, V. V., & Lambert, D. L. 1990, ApJS, 72, 387
Sneden, C. 1973, ApJ, 184, 839
Strassmeier, K. G., & Schordan, P. 2000, AN, 321, 277
Tabernero, H. M., Montes, D., & González Hernández, J. I. 2012, A&A,
  547, A13
Takeda, Y., Ohkubo, M., Sato, B., Kambe, E., & Sadakane, K. 2005, PASJ,
  57, 27
Takeda, Y., Sato, B., & Murata, D. 2008, PASJ, 60, 781
Taniguchi, D., Matsunaga, N., Kobayashi, N., et al. 2018, MNRAS,
Tody, D. 1993, in ASP Conf. Ser. 52, Astronomical Data Analysis Software
  and Systems II, ed. R. J. Hanisch, R. J. V. Brissenden, & J. Barnes (San
  Francisco, CA: ASP), 173
Van Hoof, P. A. M. 2018, Galax, 6, 63
Wright, K. O., & Jacobson, T. V. 1965, PDAO, 12, 373
Yuk, I.-S., Jaffe, D. T., Barnes, S., et al. 2010, Proc. SPIE, 7735, 77351M
```